THE JOURNAL OF PHYSICAL CHEMISTRY B

Article

pubs.acs.org/JPCB

Microscopic Origin of the Deviation from Stokes–Einstein Behavior Observed in Dynamics of the KSCN Aqueous Solutions: A MD Simulation Study

Qiang Zhang,[†,∥] Wenjun Xie,[‡] HongTao Bian,[§] Yi Qin Gao,*[,‡] Junrong Zheng,*[,§] and Wei Zhuang*[,†]

[†]State Key Laboratory of Molecular Reaction Dynamics, Dalian Institute of Chemical Physics, Chinese Academy of Sciences, Dalian 116023, Liaoning, People's Republic of China

[‡]College of Chemistry and Molecular Engineering, Beijing National Laboratory for Molecular Sciences, Peking University, Beijing 100871, China

[§]Department of Chemistry, Rice University, Houston, Texas 77005, United States

[∥]Department of Chemistry, Bohai University, Jinzhou 121000, China

ABSTRACT: Molecular dynamics simulations were carried out to investigate the microscopic origin of the deviation from Stokes–Einstein behavior observed in the dynamics of KSCN aqueous solutions. When the solution becomes more concentrated, the rotational mobilities of SCN^- and water bifurcate significantly as also observed in the experimental ultrafast infrared measurements. The translational mobilities of different components, on the other hand, have similar concentration dependences. Furthermore, when concentrating the solution, the mobilities increase slightly first and then reduce afterward. Our simulations revealed that these phenomena observed in the dynamics originate from the ion assembling in the solution. The RDF and pair residence time analysis further suggest the ion pairing effect has significant contribution to the ion assembling. Results herein thus provide a microscopic insight on the origin of the ion assembling phenomenon and its connection with various experimentally observable dynamical phenomena in the ionic solutions.

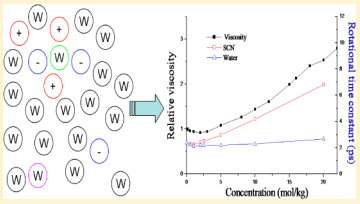

I. INTRODUCTION

Ionic aqueous solution widely exists on earth. It makes up the dominant part of the water bodies on this planet, and forms the main constituent of most living organisms. Study of ionic solutions has great significance in the fields including chemistry, biology, medicine, energy, and environmental sciences.[1−5] Understanding and exploiting the physical processes in salt solutions require a comprehensive knowledge of phase equilibria and kinetics in these systems at a broad range of concentrations.[1−25]

Models such as the Pitzer equations[26] provide a macroscopic means to calculate the thermodynamics properties of ionic solutions using the osmotic data. The predictions show excellent agreement with the experiments in the solutions with the concentration up to 6 mol/kg.[26,27] Molecular interpretation of the complex concentration and ion type dependences of these thermodynamics data, however, requires the investigations descending to the microscopic level.

An important step for studying the microscopic physics in the ionic solutions is to understand how the ions distribute in these systems. Traditional electrolyte solution theory considers the electrolytes to be completely dissociated into free cations and anions in the solution.[6,28,29] On the basis of this picture, Debye–Huckel and Onsager theories achieved the monumental success in explaining the experimental data at the dilute solutions. At higher concentrations, however, there is a non-negligible possibility of finding an ion with opposite charge inside the first solvation shells of the central ion.[30−43] An important, but not yet clearly addressed, issue is how the microscopic dynamics in the solution is influenced by this ion neighboring phenomenon.

In a recent work, we monitored the rotational dynamics of both water molecules and SCN anions in the KSCN solutions using the ultrafast vibrational energy exchange and anisotropy measurements.[44,45] As the concentration increases, a deviation from the Stokes–Einstein behavior[46,47] is observed: the thiocyanate's rotational mobility changes proportionally to the viscosity and much more significantly compared with the rotational mobility of the water molecules. Furthermore, the rotational mobilities of both components demonstrate a non-monotonic concentration dependence. As the solution becomes more concentrated, the rotational mobilities decrease first, minimize at 1−2 mol/kg, and increase afterward.

While they presented vivid evidence on the deviation from Stokes–Einstein–Debye behavior for the rotational dynamics in the ionic solutions,[46,47] our observations also raised several questions: What is the origin of this deviation in the rotational dynamics? What is the physics underlying the non-monotonic concentration dependence? Furthermore, although not detectable by the ultrafast infrared techniques, do the deviation and non-monotonicity also exist in the translational motions? To

Received: January 14, 2013
Revised: February 8, 2013
Published: February 17, 2013

investigate these issues, a quantitative theoretical investigation is desired.

In the present work, molecular dynamics simulations were employed to study the microscopic structure and dynamics in the KSCN solutions. A significant amount of ion assemblies were found in the simulation results, which is consistent with previous observations in the vibrational energy transfer experiment.[44] The residence time and radial distribution function analysis suggest that ion pairing[1] plays an important role in the formation of the assemblies. Simulations nicely reproduced the deviation from Stokes−Einstein behavior and non-monotonic feature observed in the experimental rotational mobilities. We also demonstrated that the translational mobilities have less significant deviation from Stokes−Einstein−Debye behavior compared with the rotational ones. Further analysis suggested that ion assembling is an important reason for the deviation and non-monotonicity observed. Finally, by adding other salts, such as KF and KI, into the system, significant changes of the microscopic dynamics can be induced. This is caused by the different relative affinities of F^- and I^- with other components in the solution system.

The manuscript is organized as follows: the simulation methods are discussed in section II, which is then followed by the results and discussion.

II. METHODS

Molecular dynamics simulations were carried out for the KSCN aqueous solution systems at different concentrations (0.5, 1.0, 2.0, 2.5, 5, 10.0, and 20 mol/kg). The SPC/E model[48] was used for the water molecules. In our work, the potassium ion potential is adopted from the Dang series, since it is the most popular non-polarizable ion force field[49,50] and usually used as a benchmark for ion model improvement.[51] The Dang model is developed to be consistent with the SPC/E water model. It is the main reason why we chose the SPC/E model, which is indeed a popular water model itself. The ion parameters were taken from the previous works and listed in Table 1. The

Table 1. The Force Field Parameters

	atom	q (e)	σ (Å)	ε (kJ·mol^{-1})
SPC/E[47]	Ow	−0.8476	3.166	0.650
water	Hw	0.4238	0.000	
	S	−0.0.56	3.52	1.5225
SCN^- [a]	C	0.16	3.35	0.425
	N	−0.58	3.31	0.310
K^+ [50]		+1.0	3.33	0.42
F^-		−1.0	3.12	0.75
I^-		−1.0	5.17	0.42

[a]Vincze, Á.; Jedlovszky, P.; Horvai, G. *Anal. Sci.* **2001**, *17*, i317.

cubical periodic boundary boxes were used in the simulations. The 1:1:10 (KF:KI:KSCN) and 1:1:10 (KI:KI:KSCN) solutions were also simulated to investigate the mixed ion effect. The simulation boxes were constructed as the ratio in Table 2.

The bond lengths and angles of water and SCN^- were constrained at the equilibrium values (1.69, 1.15, and 1.0 Å for the bond lengths of S−C, N−C, and O−H; 109.47 and 180° for the bond angles of SCN^- and water) by the SHAKE algorithm.[52] The Lorentz−Berthelot rules[53] were used for the current combined Lennard-Jones potential parameters. For each sample, a 5 ns NPT ensemble equilibration was carried

Table 2. The Details of the Simulation Boxes

concentration (mol/kg)	number of KSCN	number of mixed ions	number of water
0.5	12		1176
1	24		1176
2	46		1154
2.5	56		1122
5	110		1090
10	200		1000
20	416		1000
1 (KF):1 (KSCN)	110	110 (KF)	1090
1 (KI):1 (KSCN)	110	110 (KI)	1090

out to generate the proper size of the simulation box; it was followed by a 10 ns NVE ensemble simulation used to calculate the dynamic properties. For each NPT simulation, the temperature is weakly coupled to a bath with the Nosé−Hoover thermostats[54,55] at 298 K with a relaxation time of 0.1 ps. The weak coupling Berendsen scheme was used to control the system pressure at 1 atm with a coupling time constant of 1 ps.[56] The equations of motion were integrated using the velocity Verlet integration scheme[53] and a time step of 2 fs. The long-range Coulombic forces are calculated using the particle-mesh Ewald method.[57] The non-bonded van der Waals interactions are truncated at 12 Å using the switching functions. Minimum image conditions[53] were used. The simulation trajectories are saved every 100 fs. All simulations are performed using the Tinker simulation code.[58]

The densities from our simulations are listed in Table 3. The simulation densities are slightly higher than those from

Table 3. The Densities of KSCN Water Solutions from Simulations and Experiments

concentration	MD density	concentration	exp. density
0.5	1.0528	0.5307	1.0218
1	1.0853	1.0087	1.0434
2	1.1212	2.0184	1.0885
2.5	1.1458	2.5124	1.1103
5	1.2416	3.9644	1.1728

experiments.[59] However, the density increases with concentration, which is consistent between the simulations and experiments. The discrepancy between the simulations and experiments is possible due to the force field parameters used. The previous work suggests that the SPC/E water model is not appropriate for the very concentrated solutions.[60]

Ion Assembly and Hydrogen Bond Definitions. An ion assembly is defined as the following: (i) every ion X (X = SCN^-, I^-, F^-, or K^+) is connected to at least one ion Y of the opposite charge; two ions are said to be connected if they are separated by a distance R_{X-Y} smaller than the separation d corresponding to the first minimum of the pair radial distribution function. ($R_{X-Y} < d$ Å for K−S (d = 4.0), K−N (d = 3.5), K−F (d = 3.4), and K−I (d = 4.5) pairs); (ii) every ion can be reached from any other ion within the assembly through a path of consecutive connections. The total number of all the ions in each ion assembly is defined as the size of the assembly. Note this definition of the assembly contains no information about the lifetime. An ion assembly defined this way can be due to the instantaneous thermal fluctuation, or it can be an assembly with longer lifetime and caused by more complex energetic reasons. A thorough study of the lifetime

dx.doi.org/10.1021/jp400441e | J. Phys. Chem. B 2013, 117, 2992−3004

Table 4. The Coordination Numbers at the Different Concentrations (mol/kg)[a]

	20	10	5	2.5	2	1	0.5	KF	KI
N_{K-Ow}	2.74	3.89	5.14	6.11	6.16	6.79	6.96	5.45	3.61
N_{K-S}	2.20	1.68	1.12	0.61	0.60	0.29	0.16	0.96	0.79
N_{K-N}	1.97	1.44	0.84	0.47	0.43	0.17	0.14	0.80	0.71
N_{K-F}								0.25	
N_{K-I}									1.49
N_{S-K}	2.20	1.68	1.12	0.61	0.60	0.29	0.16	1.92	1.58
N_{N-K}	1.97	1.44	0.84	0.47	0.43	0.17	0.14	1.60	1.42
N_{F-K}									
N_{I-K}									2.99
N_{F-Ow}								6.14	
N_{I-Ow}									3.45
N_{OwOw}	3.15	3.94	4.47	4.83	4.95	5.12	5.22	4.42	3.77
N_{S-Ow}	2.07	2.78	3.45	3.95	3.96	4.21	4.32	2.85	2.72
N_{N-Ow}	1.86	2.51	3.18	3.53	3.56	3.79	3.79	2.56	2.41

[a]N_{X-Y} denotes the coordination number of Y around the central atom X by the integration from 0 to the first minimum of the pair radial distribution function.

Table 5. The Diffusion Constants (10^{-5} cm^2/s), Rotational Correlation Times (ps), and Residence Times (ps) of Water and Ions, as Well as the Corresponding Values of Their Subspecies in the KSCN Solutions and Mixing Solutions[a]

C (mol/L)	20	10	5	2.5	2	1	0.5	0	5 (KF)	5 (KI)
D mean	0.70	1.49	2.00	2.33	2.47	2.62	2.59	2.44	0.47	1.32
D water	1.08	1.80	2.19	2.44	2.53	2.64	2.61	2.44	0.56	1.61
D K	0.28	0.80	1.14	1.43	1.59	2.30	2.20		0.30	0.63
D SCN	0.30	0.73	1.10	1.49	1.85	1.79	1.61		0.26	0.51
D F				1.26					0.19	
D I										0.52
τ_2^{OH} mean	2.67	2.29	2.17	2.17	2.17	2.15	2.23	2.38	8.21	2.60
τ_2^{SCN} mean	6.81	4.18	2.98	2.50	2.39	2.28	2.28		8.47	4.49
τ_2^{OH} PWB	2.00	2.04	2.02	2.12	2.14	2.14	2.23		3.96	2.24
τ_2^{OH} PB	2.41	2.26	2.19	2.20	2.19	2.11	2.19		4.99	2.55
τ_2^{OH} TB	2.28	2.14	2.20	2.24	2.22	2.27	2.32		5.51	2.51
τ_2^{OH} BPT	2.87	2.50	2.32	2.27	2.28	2.20	2.27		6.95	2.82
τ_2 PWB SCN	3.22	2.36	2.29	2.23	2.18	2.21	2.22		5.49	2.70
τ_2 PB SCN	6.84	4.29	3.09	2.63	2.54	2.42	2.36		8.53	4.60
τ_S PWB water	1.48	3.14	5.01	9.09	13.11	25.4	51.4		4.15	4.07
τ_S PB water	0.84	1.49	1.85	2.54	2.75	3.15	3.52		4.31	1.64
τ_S TB water	1.94	2.15	2.26	2.16	2.19	2.15	2.08		1.99	1.80
τ_S BPT water	10.01	5.58	2.57	1.61	1.51	1.27	1.24		4.41	2.17
τ_S PWB SCN	3.30	6.00	9.53	15.29	24.11	41.1	74.9		4.20	4.62
τ_S PB SCN	76.46	43.66	13.83	8.46	6.76	2.97	2.38		43.43	24.72
τ_R W−W	9.23	7.04	6.33	6.06	5.98	5.97	6.04	6.15	17.3	7.52
τ_R K−W	15.66	11.70	9.84	9.00	8.54	7.97	8.06		26.6	12.82
τ_R S−W	8.4	5.66	4.62	4.3	4.2	3.97	4.27		10.14	5.97
τ_R N−W	10.22	7.39	6.02	5.49	5.62	5.38	5.26		13.15	7.76
τ_R K−S	27.06	17.83	12.96	10.03	9.02	7.76	8.28		26.76	17.29
τ_R K−N	29.81	18.68	11.69	9.08	7.81	7.33	7.48		29.85	17.41

[a]W−W, K−W, S−W, N−W, K−S, and K−N atom pairs defined to obtain the water−water, K−water, SCN−water, and K−SCN pair residence times.

distribution and the energetic origin of these ion assemblies are beyond the scope of this manuscript.

For a specific ion X, if the separation R_{X-Y} between X and one water or ion Y is not larger than d_{X-Y}, which corresponds to the first minimum of the RDF (d_{Ow-Ow} = 3.5, d_{N-Ow} = 3.4, d_{S-Ow} = 3.6, d_{K-Ow} = 3.6, d_{F-Ow} = 3.2, d_{I-Ow} = 4.0, d_{K-S} = 4.0, d_{K-N} = 3.5, d_{K-F} = 3.4, and d_{K-I} = 4.5), they are considered to be in the first solvation shell of X. The number of ion or water in the solvation shell of X is defined as the coordination number of X in Table 4.

Two water molecules are considered to be hydrogen bonded if the distance between their oxygens is R_{OwOw} < 3.5 Å and the angle is θ_{HOwOw} < 30° (O_w, water oxygen atom; H_w, water hydrogen atom).

Subspecies Definition. In the pure KSCN aqueous solutions, we defined four categories of water molecules according to the surrounding environments. (1) Pure water bound (PWB): there are only water molecules in its first solvation shell. (2) Potassium bound (PB): the first solvation shell has only K^+ besides water. (3) Thiocyanate bound (TB):

dx.doi.org/10.1021/jp400441e | J. Phys. Chem. B 2013, 117, 2992−3004

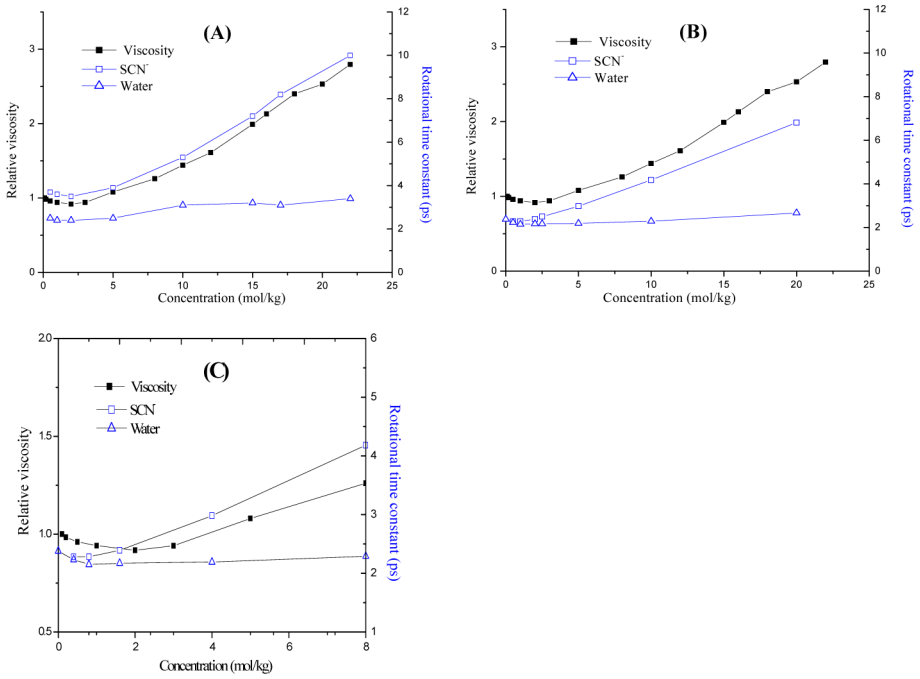

Figure 1. (A) The concentration dependent viscosities (black) and rotational correlation times of SCN^- anions and D_2O (blue) in the KSCN aqueous solutions detected in the experiments; (B) the corresponding rotational correlation times from MD simulations, compared with the experimental viscosity; (C) the zoomed-in figure of part B at a low range of concentration.

the first solvation shell has only SCN^- besides water. (4) Bridge between potassium and thiocyanate (BPT): the first solvation shell has at least one K^+ and one SCN^-. In the KSCN solutions with additional F^- or I^- ions, two more subspecies are defined. (5) Halide ions bound (HB): the first solvation shell has only F^- (I^-) besides water molecules. (6) Bridge between potassium and halide ions (BPH): the first solvation shell has at least one K^+ and one F^- (I^-).

Similarly, thiocyanate ions and potassium ions can be separated into two types in the following way. (1) Pure water bound (PWB): the first solvation shell contains only water molecules. (2) Ion bound (IB): the first solvation shell contains at least one ion.

Pair and State Residence Time. The time dependent pair correlation functions, $R(t)$, are employed to calculate the residence times for the water−water pair (W−W), ion−ion (SCN−K pair: N−K and S−K), and ion−water pairs (SCN−water pair: N−W and S−W; K−water pair: K−W).[21,61] $R(t)$ represents the probability that one pair, X and Y, exists at $t = 0$ is still intact at a later time t

$$R(t) = \langle h(t)h(0)\rangle/\langle h(0)\rangle \tag{1}$$

$h(t)$ is the population operator. $h(t) = 1$ when the distance of the pair is smaller than the d_{X-Y}, and $h(t) = 0$ otherwise. The angular brackets denote the ensemble average.

To calculate the continuous pair residence time τ_C, we set all $h\ (t' > t) = 0$ once the pair distance is longer than d_{X-Y} at the moment t. $R(t)$ is then calculated and fitted with a double exponential decay function. The relaxation time of the slower procedure is defined as τ_C. To exclude the transient escape of a labeled pair, we also calculated the intermittent pair residence times τ_R in a similar way. Different from τ_C, the transient escape of the pair, with the leaving time shorter than 2 ps, is allowed in the calculation of τ_R.[62,63] τ_C and τ_R for different pairs are presented in Table 5.

A similar routine can be applied to extract the "state residence time" τ_S of water and SCN^- subspecies. Here, $h(t) = 1$ when the labeled water and ion meets the criteria of subspecies definition at evolution time t, and $h(t) = 0$ otherwise. The transient departure (<2 ps) from the current state is allowed for τ_S.

Rotational Correlation Time. The second-order reorientation correlation function $C^\alpha(t)$ of a molecule or ion in a solution is described as a second-order Legendre polynomial[64−67] along a molecular axis α:

$$C(t) = \frac{1}{2}\langle 3[\mathbf{e}(t)\cdot\mathbf{e}(0)]^2 - 1\rangle \tag{2}$$

where $\mathbf{e}$ is a unit vector pointing along this axis. In general, $C^\alpha(t)$ shows an exponential decay

$$C^\alpha(t) = A\exp\left(-\frac{t}{\tau_2}\right) \tag{3}$$

where A is a constant. τ_2 is the rotational correlation time of this molecular axis α and is related to the experiment measurements.[64] The rotational correlation times were calculated by fitting in the time interval for which $\ln(C^\alpha(t))$ decreases linearly.[65−67]

We can, similarly, define the rotational correlation function $C^\alpha(t)$ for a specific subspecies from eq 2, with only the requirement that the target water or SCN^- belongs to this subspecies at $t = 0$, regardless of the following status of the target molecule at $t > 0$.

Diffusion Constant. The self-diffusion coefficient D can be derived from the time-dependent mean square displacements of the labeled molecule or ion in the solutions, according to the Einstein relation[53,63]

$$D = \lim_{t\to\infty}\frac{\langle|\mathbf{r}(t) - \mathbf{r}(0)|^2\rangle}{6t} = \lim_{t\to\infty}\frac{T(t)}{6t} \tag{4}$$

dx.doi.org/10.1021/jp400441e | J. Phys. Chem. B 2013, 117, 2992−3004

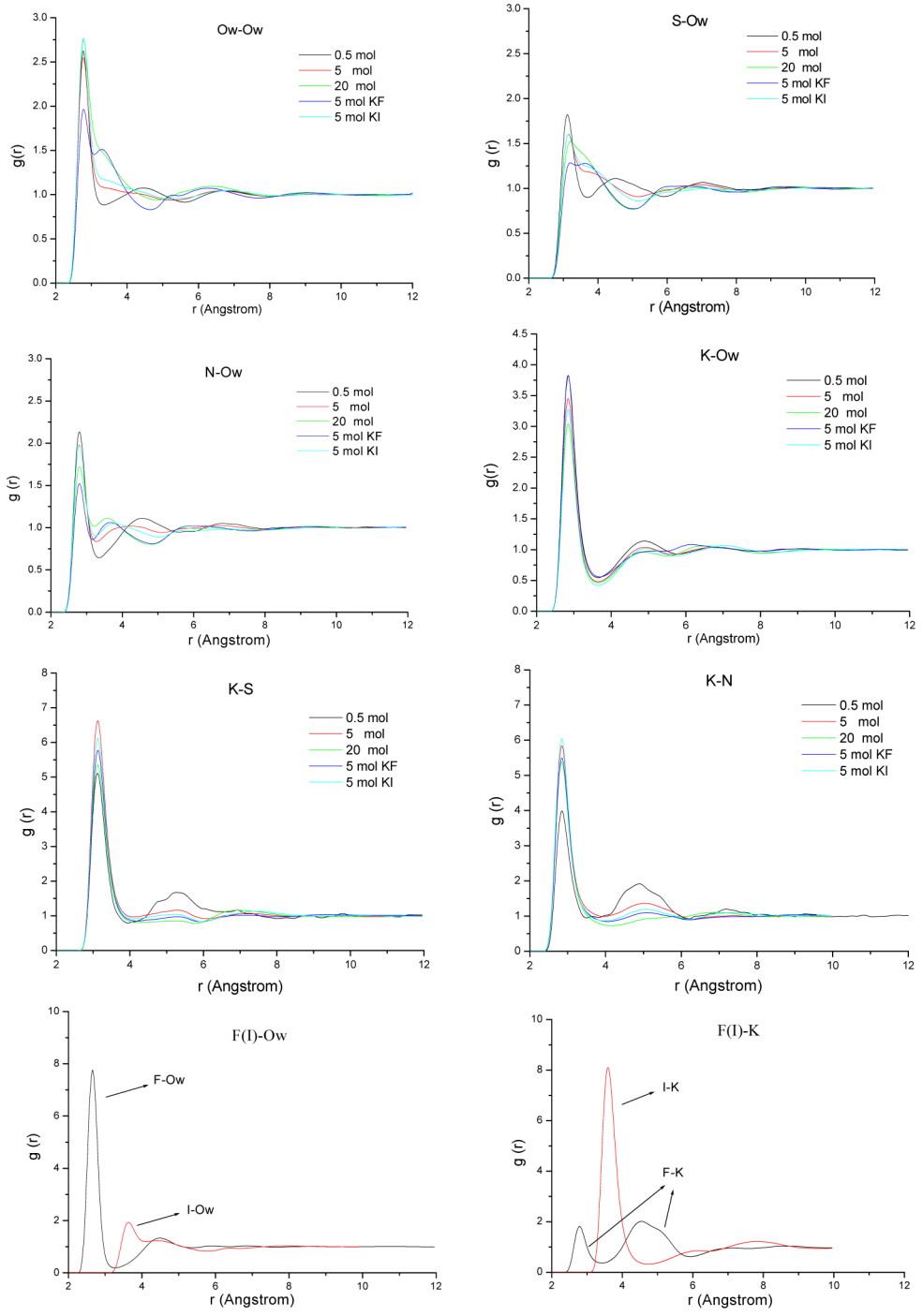

Figure 2. The radial distribution functions for the Ow−Ow, N−Ow, S−Ow, K−Ow, F−Ow, I−Ow, F−K, and I−K pairs.

$\mathbf{r}(t)$ is the position vector of the molecular or ion center of mass at time t, and the averaging is performed over all molecules or ions of the same type. $T(t)$ is the time-dependent mean square displacements. The diffusion constant of a solution is calculated as the mean square displacements over all molecules and ions averagely in the solution.

The time-dependent mean square displacements of the subspecies, $T(t)$, are used to interrogate the mobilities of subspecies. If one water or ion in the solutions belongs to one type of its subspecies at $t = 0$, the time-dependent mean square displacements are traced forward regardless of the state following it. Similar as in the discussion of the subspecies rotation, it is only meaningful to discuss the behavior of $T(t)$ for a certain subspecies when the time is shorter than its residence time.

III. RESULTS

(A). Rotational Mobility Observed in Simulation and Experiment. The concentration dependences of the rotational correlation times of SCN^- and water in the simulation are presented in Figure 1B and compared with the experimental anisotropy and viscosity measurements in Figure 1A. The simulation resembles most of the experimental results, including the bifurcating between the rotational mobilities, the strong correlation of SCN^-'s rotation with the viscosity, and

dx.doi.org/10.1021/jp400441e | J. Phys. Chem. B 2013, 117, 2992−3004

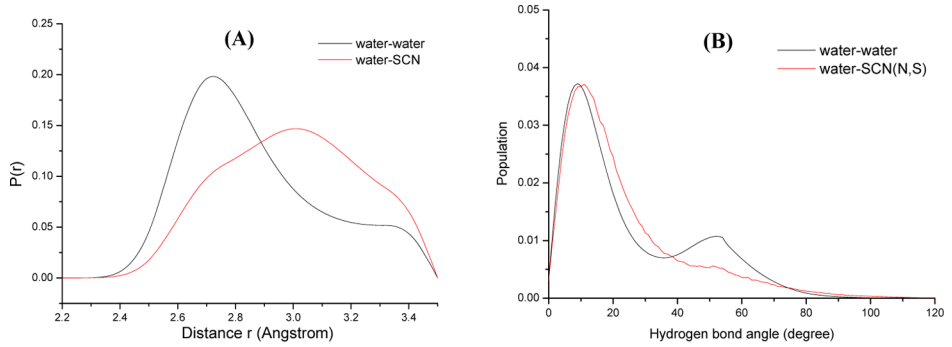

Figure 3. The distribution of the hydrogen bond lengths and angles for the water−water and water−SCN. Only the pairs with the distance R_{X-Y} less than critical separation d (d_{Ow-Ow} = 3.5 Å, d_{N-Ow} = 3.4 Å, d_{S-Ow} = 3.6 Å, as defined by the first minimum of the RDFs) and the hydrogen bond angle less than 50° are included in the calculation. The hydrogen bond angle is defined as the H−O−O angle for the one H atom of the four that makes the smallest angle as the following reference: Sharp, K. A.; Vanderkooi, J. M. *Acc. Chem. Res.* **2010**, *43*, 231−239.

the non-monotonic concentration dependence of water rotational mobilities in Figure 1C. For the thiocyanate, although the simulation does not precisely reproduce the experimentally observed small augmentation of rotational correlation time at lower concentrations, the simulated rotational mobility follows a fairly flat curve which does not deviate much from the experimental result. The minor mismatch may be due to the force field used.

(B). Structure and Ion Assembly. The radial distribution functions (RDF) of Ow−Ow, N−Ow, S−Ow, K−Ow, K−N, and K−S pairs in the pure KSCN solutions are shown in Figure 2. The first peak of the Ow−Ow RDF only changes slightly with the concentration, while the second peak is weakened significantly due to the disruption of the second solvation shell of water molecules by the ions.[68] Appearance of the peak at about 3.5 Å indicates the probability of two waters appearing in the first solvation shell of the same ion increases. The maxima of the first peaks of N−Ow and S−Ow RDFs are 2.8 and 3.2 Å, respectively. The association between the SCN^- and water weakens at higher concentrations, which can be found from the coordination numbers of N_{S-Ow} and N_{N-Ow} in Table 4. The association structures between water and SCN^- discussed herein is consistent with the previous simulations.[70]

The length and angle distribution of two types of hydrogen bonds, water−water and water−SCN pairs, are presented in Figure 3. The water−water pair has smaller average lengths and angles as well as a narrower distribution compared with the water−SCN pair, as can be observed in Figure 3.

For the different water subspecies, the water−water hydrogen bond numbers attached to a single water molecule are shown in Figure 4. The average number decreases more rapidly than that for each subspecies. The number of the attached hydrogen bond is the largest for the PWB water and the smallest for the BPT water. The average hydrogen bond number is determined by the PWB type and BPT water at low and high concentration, respectively.

The first peaks in the RDFs of K−N and K−S are significantly higher than the ion−water pairs. The coordination number of SCN^- to K^+ increases from 0.30 to 4.17 as the concentration changes from 0.5 to 20 M. The experimental values are 0.2 and 0.9 at 0.6 and 2.9 M.[68] The average assembly size and the ratio of ions in the assemblies increase with concentration (Figures 5 and 6). For the solution with the lowest concentration of 0.5 mol/kg, a K^+ has 6.96 waters in its first solvation shell averagely (5.9 water at 0.6 mol/kg from ref 68), while a SCN^- has 8.11 waters, including 3.79 for the N

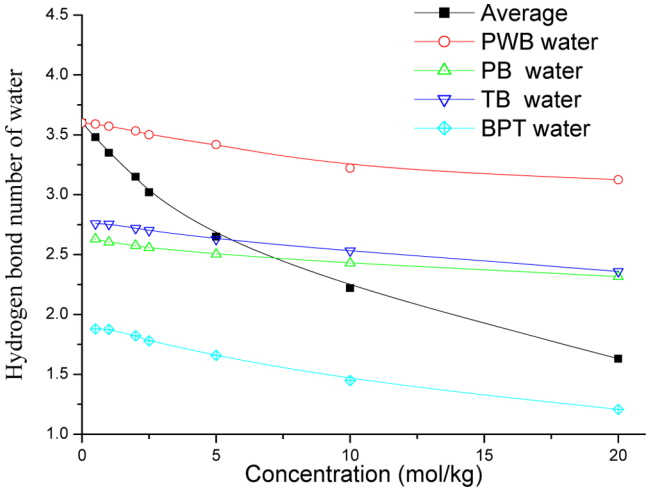

Figure 4. The average number of water−water hydrogen bonds connected with each water molecule for different subspecies.

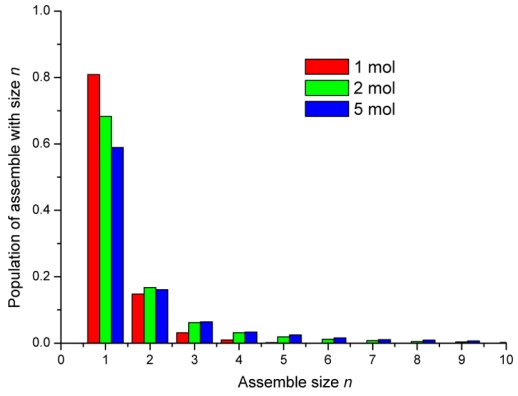

Figure 5. The population of the ion assemblies in the KSCN solutions at different concentrations.

terminal (3.1 at 0.6 mol/kg from ref 68) and 4.32 for the S terminal. Theoretically, the ions can be fully dissociated in the solution at 2 mol/kg according to the ratio of two components (1KSCN:25water) and the coordination numbers at 0.5 mol/kg. However, 60% of ions form assemblies at 2 mol/kg. The facts above show that SCN^- and K^+ thus have a high tendency to pair with each other.

There are significantly higher first peaks for the radial distribution functions of the K−N, K−S, and K−I ion pairs

dx.doi.org/10.1021/jp400441e | J. Phys. Chem. B 2013, 117, 2992−3004

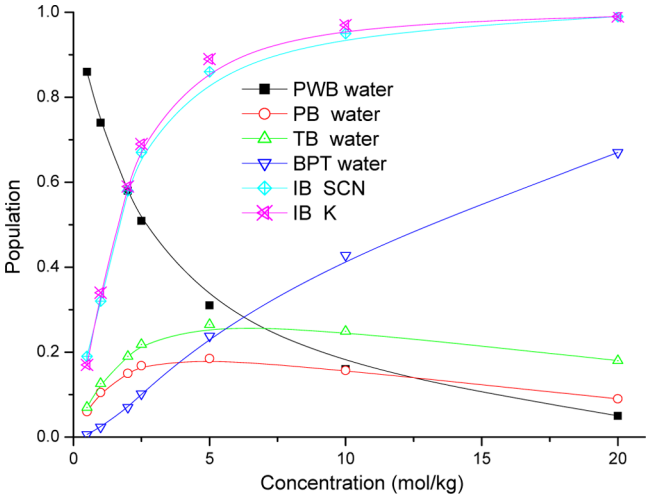

Figure 6. The populations of the different subspecies of water and ions at different concentrations.

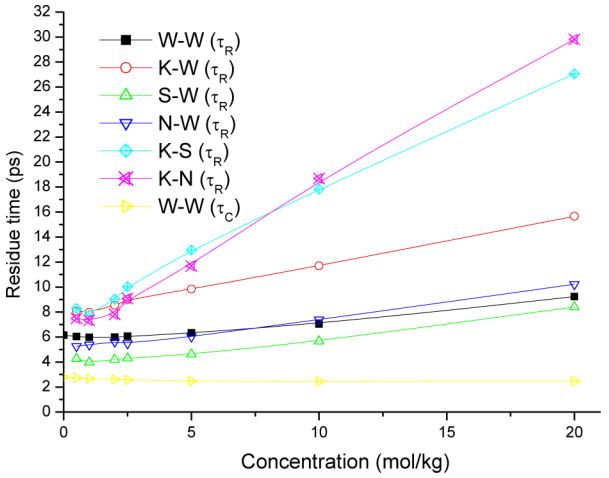

Figure 7. Residence times, τ_R, for the water−water (W−W), K−water (K−W), SCN−water (residence times for S−W and N−W atom pairs), and SCN−K (residence times for the S−K and N−K atom pairs). The continuous residue times, τ_C, for the water−water are also presented.

than that of the K−F pair, which means that the CIP (contact ion pair) configures are more favorable for the former ones than the last (Figure 2). K−F pairs, on the other hand, favor the SSIP (single solvent separated ion-pair) structures,[2,42,69,70] as suggested by a higher and broader second association peak in the range 4−6 Å (Figure 2). A strong peak can be found at 2.65 Å for the F−Ow pair and a weaker peak at 3.65 Å for the I−Ow pair, which indicates a higher water affinity of F^- compared with I^-. Adding KI has a similar effect to increasing the concentration of KSCN. The total coordination number of K^+ is 6.60 (3.61 for water oxygen, 0.79 for SCN^- sulfur, 0.71 for SCN^- nitrogen, and 1.49 for iodine), which is similar to that in the KSCN solution at 10 mol/kg (3.89 for water oxygen, 1.68 for SCN^- sulfur, and 1.44 for SCN^- nitrogen). The only difference is that some SCN^- in the ion assemblies at 10 mol/kg is replaced with the iodine ions. The mixed ion assemblies are formed in the mixed solutions. The local environment of SCN is also similar to that in the KSCN solution of 10 mol/kg. This can be deduced from the coordination numbers and components of sulfur and nitrogen atoms in Table 4.

In the solution of KSCN:KF:water, 87, 98, and 41% of K^+, SCN^-, and F^- are assembled, respectively, while, in the KSCN:KI:water solution, the ratio is 97, 95, and 97% for K^+, SCN^-, and I^-. Both systems have a higher assembled ratio of SCN^- compared with the pure KSCN (5 mol) solution, in which 89% of K^+ and 86% of SCN^- were assembled. The big difference between the assembly ratio of F^- and I^- is due to the higher water affinity of the F^- compared with I^-.

The concentration-dependent populations of different subspecies of water, K^+, and SCN^- are shown in Figure 6. The populations of the ions in the assemblies increase drastically within the range 0.5−5 mol/kg. The ratio of PWB water decreases and the population of the BPT water increases monotonically with concentration. One maximum can be observed at a concentration of 5 mol/kg for the PB or TB water.

(C). Pair Residence Time. The residence times for the water−water (W−W), K−water (K−W), SCN−water (N−W and S−W), and K−SCN (K−N and K−S) pairs at different concentrations are presented in Figure 7 and listed in Table 5. The residence times, τ_R, of water−water and water−SCN pairs (either S or N atom) are shorter than those of K−water and K−CN pairs and have relatively minor variations with salt concentration. A minor monotonous decrease is found for the continuous residence times τ_C for the water−water pair. The difference between the τ_C and τ_R of water−water residence time suggests that transient breaking and reforming for the water−water pair happen more frequently at the higher concentrations. The residence times of S−W and N−W pairs are slightly shorter than those for the water−water pair at low and median concentration and increase relatively faster afterward.

In the KF:KSCN:water solution, the residence times of the W−W, K−W, S−W, N−W, S−K, and N−K pairs are 17.3, 26.6, 10.14, 13.15, 26.76, and 29.85 ps, respectively, significantly higher than the corresponding values in the KSCN solution at any concentration. In the KI:KSCN:water solution, a similar residence time was found for different pairs as in the KSCN solution at 10 mol/kg (Table 5).

(D). State Residence Time. The state residence times, τ_S, for different subspecies of water and SCN^- are presented in Figure 8. The PWB states have the longest residence time for

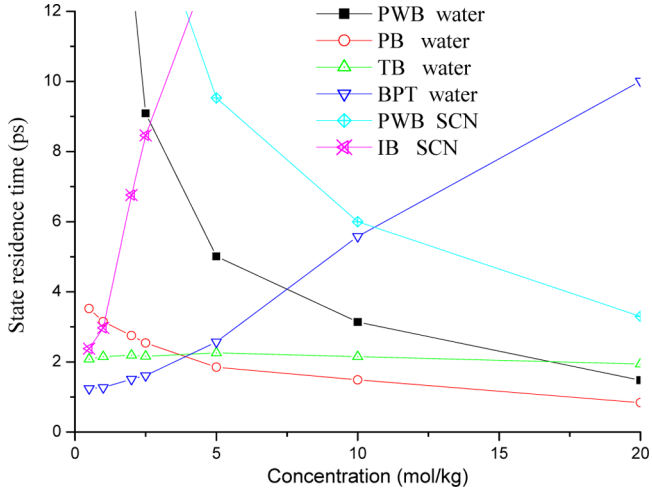

Figure 8. The state residence times of the subspecies of water and SCN^- at different concentrations.

dx.doi.org/10.1021/jp400441e | J. Phys. Chem. B 2013, 117, 2992−3004

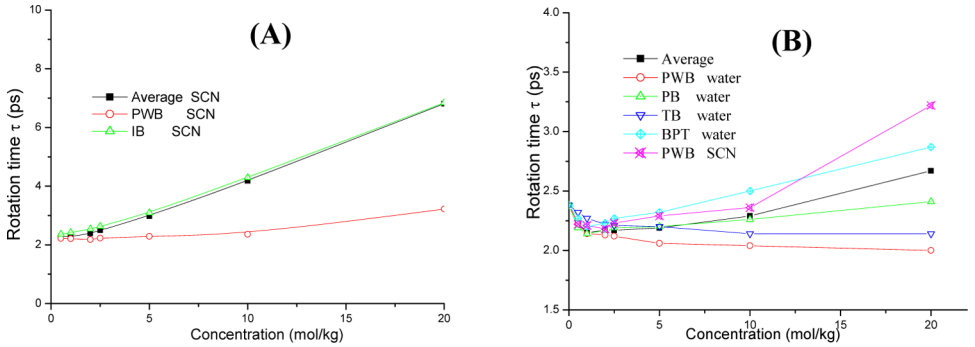

Figure 9. (A) The rotational correlation times of the SCN^- in average and two subspecies PWB and IB. (B) The rotational correlation times of water in average and four subspecies. The subspecies for water and SCN are defined in section II. For comparison, the rotational correlation time of PWB SCN is also plotted here.

both water and SCN^- at low concentrations, while the BPT water and IB SCN^- are the most stable states at higher concentrations. The state residence times of the PWB water and SCN^- both decrease rapidly at lower concentration. The former is a little higher than the latter at all concentrations. The state residence times of the IB SCN^- increases more sharply than that of BPT water.

(E). Rotational Mobility. The concentration dependence of the rotational correlation times for both SCN^- and water molecule are demonstrated in Table 5 and Figure 9. For SCN^-, the overall rotational correlation time correlates strongly with IB SCN when the concentration is above 1 mol/kg and with PWB SCN^- when the concentration is below that. The rotational mobilities of PWB and IB SCN^- diverge significantly at higher concentrations. A very weak decrease can be found from 0 to ~2 mol/kg for PWB SCN^-.

The rotational correlation times of water in average, PB water and BPT water decrease with concentration at low concentrations, approach minima at about 1 mol/kg and increase monotonously afterward. The rotational correlation times of the PWB water and the TB water decrease monotonously with concentration.

A clear anisotropic rotational behavior is observed for the water (Figure 10) at a low concentration, such as 0.5 mol/kg, which is consistent with the previous study.[71] Water molecules rotate a little faster along the dipole direction (2.05 ps) than the O−H bond direction (2.23 ps). A little slow rotation along the dipole moment vector (2.17 ps) for the PB water than the PWB water (2.04 ps) is observed, which is also consistent with the previous studies.[73] There is no evident difference for the rotation of water in the different environments along the O−H bond and the dipole direction due to the weakly hydrated effects for the K^+ and SCN^-. A little faster decay at short times (inset of Figure 10) is observed for the rotational correlation function of TB water than other cases.

The rotational correlation times of water and SCN^- in the 1:1:10 (KF:KSCN:water) solution are 8.21 and 8.47 ps averagely, and correspondingly 2.60 and 4.49 ps in the 1:1:10 (KI:KSCN:water) solution and 2.29 and 4.18 ps in the 1:10 (KSCN:water) solution. The effect of KI is similar to the concentrated effect on the rotational mobility of water and ions, which can be found in Table 5.

(F). Translational Mobility. Translational mobility can be studied by the self-diffusion constants calculated by eq 4. The diffusion constant of each species in the KSCN solution is presented in Figure 11 and Table 5. The mean diffusion constant D slightly increases at the low concentration, reaches a

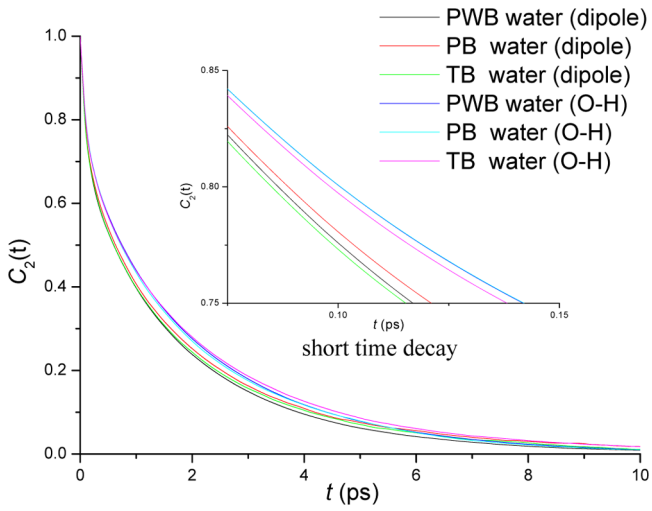

Figure 10. Anisotropic rotational correlation functions of water along the O−H bond and dipole vector in the solution with the KSCN concentration of 0.5 mol/kg. The short time decay curves are shown in the inset figure correspondingly.

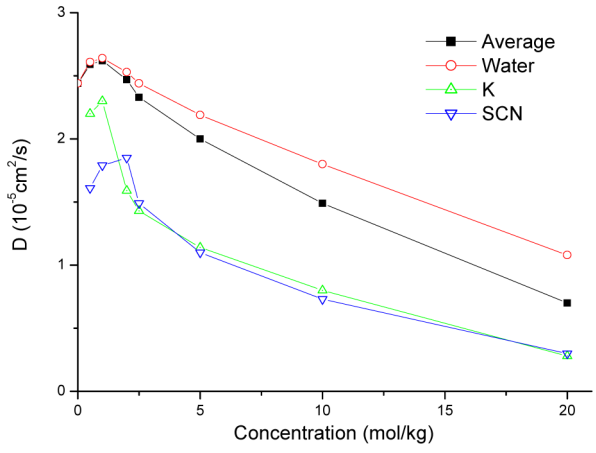

Figure 11. Diffusion constants of water, K^+, and SCN^- and the mean values at the different concentrations.

maximum at about 1 mol/kg, and decreases afterward. The diffusion constant of water has a slightly weaker correlation with the concentration compared with the ions. Water is the fastest component in the solution at any concentration. The diffusion constants of K^+ and SCN^- strongly correlate with each other as concentration higher than 2.5 mol/kg and are

dx.doi.org/10.1021/jp400441e | J. Phys. Chem. B 2013, 117, 2992−3004

close each other. The coupling translation is also found in the mixed solutions, the similar values of 0.30 and 0.26 for them in the 1:1:10 (KF:KSCN:water) solution and 0.63 and 0.51 in the 1:1:10 (KI:KSCN:water) solution. The diffusion constants of water, K^+, and SCN^- in the 1:1:10 (KF:KSCN:water) solution are much lower than those in the 1:10 (KSCN:water) solution (0.80 and 0.73 × 10^{-5} cm^2/s) and similar to those in the 1:1:10 (KI:KSCN:water) solution.

The relative translational and rotational mobilities of water at different concentrations are presented in Figure 12 and

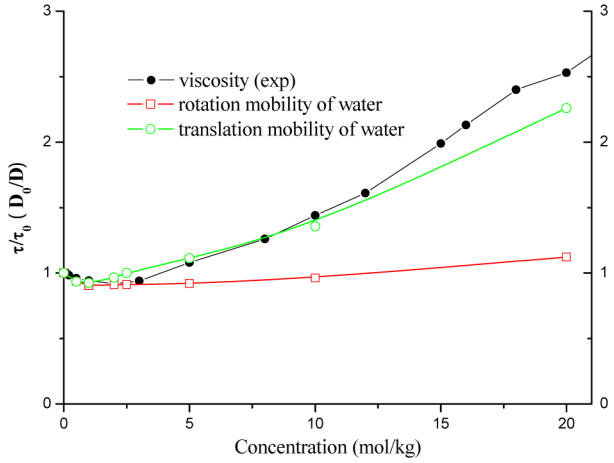

Figure 12. The relative rotational correlation times (τ/τ_0: τ_0 is the rotation time of pure water) and translational diffusion constants (D/D_0: D_0 is the diffusion time of pure water) of water compared with the experimental viscosity at different concentrations. The curves are scaled with the values in the pure water.

compared with experimental viscosity. Translational mobility has a much stronger correlation with the viscosity than the rotational mobility, which deviates from the Stokes−Einstein−Debye (SED) relation.[46,47]

The time-dependent mean square displacements $T(t)$ of the PWB water are demonstrated in Figure 13. The $T(t)$ of the PWB water in low concentration (0.5 and 1 mol/kg) solutions almost increase linearly, similar as in pure water but with a little larger displacement. As the concentration further increases, the $T(t)$ of PWB water bends at long time scale.

IV. DISCUSSION

Rotational dynamics of the water and SCN^- demonstrate a significant difference in their concentration dependences. The rotational mobility of SCN^- is more sensitive to the concentration change than that of water molecules. On the other hand, the translational motions of different components have similar concentration dependences. The translation and rotation of water molecules thus appear to have rather different concentration dependences, as also suggested by Wynne and co-workers.[72] Furthermore, a non-monotonic concentration dependence was found for the mobilities of water.

To understand the underlying structural origin of the observed deviation from the Stokes−Einstein behavior in the solution dynamics, we analyzed the local environments of ions at different concentrations. In Figure 2, the first peaks of the N−Ow and S−Ow RDFs are weaker compared with those of the Ow−Ow pair, while the first peaks of K−N and K−S RDFs are stronger than those of ion−water RDFs, which indicates that K^+ and SCN^- have a higher probability to stay next to each other instead of separated by water molecules. Further analysis in Figure 5 suggests that this cation−anion affinity causes a significant amount of ions to assemble even at the moderate concentrations, which is consistent with the recent ultrafast vibrational energy exchange measurements.[44,45] Figure 5 also demonstrates that bigger ion assemblies form as the concentration gets higher.

The ion assemblies create different local environments for both water and the ions at the microscopic level. Consistent with the hydrodynamic theory[73−79] and the recent experiments,[79,80] our simulation suggests that this diversity has significant influences on the molecular dynamics in the solution. The rotational mobilities of ions and water molecules depend on their local environments. As presented in Figure 9, at higher concentrations, the overall rotational mobility of SCN^- is largely determined by the IB SCN^-, while the overall rotational mobility of water is decided by the BPT water, whose concentration dependence is similar to the PWB SCN^- and much weaker than the IB SCN^-. Thus, the difference of the rotational dynamics happens due to the significant ion assembling in the solutions.

Naturally, for the discussion of the subspecies mobilities to be meaningful, the state residence time of the specific subspecies under investigation should be longer than the characteristic relaxation time of the processes, so that the target molecules stay, statistically, in the same subspecies during the measurement. As demonstrated in Figure 9B, at the lower concentrations, the overall rotational mobility of water is determined by the PWB water which, under this circumstance, has a much longer residence time than its rotational correlation time; this is because only a small amount of ions exist in the solution and most of the water molecules are surrounded by their peer. At higher concentrations, the BPT water determines

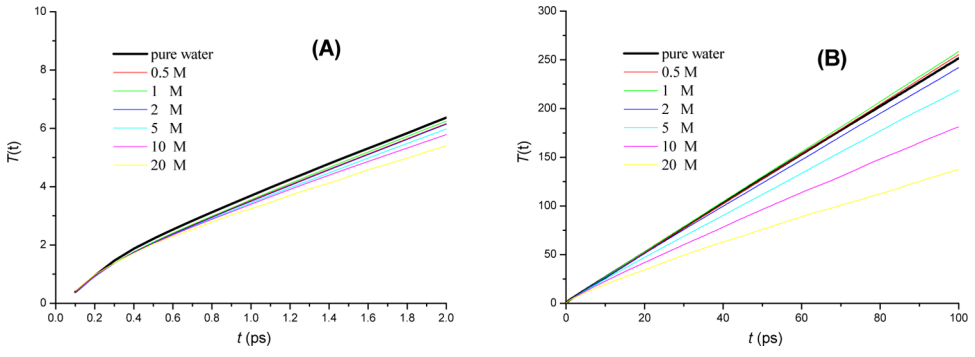

Figure 13. The time-dependent mean square displacements $T(t)$ of the PWB water at the different concentrations within (A) 2 ps and (B) 100 ps.

dx.doi.org/10.1021/jp400441e | J. Phys. Chem. B 2013, 117, 2992−3004

the overall rotational mobility; its residence time is also significantly longer than its rotational correlation time, since at these concentrations there is only a small amount of water molecules and they are most likely confined in the ion assemblies. Similar situations can be found for SCN^-; at lower concentrations the behavior is similar to the PWB SCN^-, and higher concentrations IB SCN^-, whose mobilities are well-defined under those circumstances, respectively. Our analysis of the rotational dynamics based on the subspecies contributions is thus meaningful.

The non-monotonic concentration dependence of the rotational correlation time is possibly the consequence of two competing factors: the water hydrogen bond weakening caused by ions speeds up the motions, and the confinement of the ion assemblies retards them. In the following, we discuss this by interrogating the concentration dependences of the subspecies rotational mobilities.

We first consider the rotational motions of water molecules. Two processes are expected to contribute to the rotational motion of the water molecules:[65] a faster, large-amplitude angular jump and a slower, diffusive reorientation between the hydrogen bond switches due to the coupling of the OH to the OO framework. The former is a local process that depends on the hydrogen bond exchange reaction rate,[21,64,81−83] which is strongly affected by the number of hydrogen bond acceptors nearby and the strength of the hydrogen bonds on the water molecule. The latter should be a rather long-range and collective motion dominated by the complex hydrogen bonding network in the aqueous solution, which can be affected by the weakening of hydrogen bonds at certain distance away. In our simulation, the faster short-time decay of the water−SCN hydrogen bond's rotations in Figure 10 compared with those of the water−water hydrogen bonds, as discussed in ref 83, suggests a weaker hydrogen bond. Furthermore, the hydrogen bond strength can be reflected from the librational cone size of the hydrogen bond;[83] the broader length and angle distributions of the hydrogen bond for the water−SCN (Figure 3) also suggest a weaker strength. All of these observations above, consistent with the report in the literature of SCN^- as a structure breaker,[84,85] suggest that the hydrogen bond structures of water are weakened by the SCN^-, which should result in a decrease of the rotational free energy barrier and thus a minor speeding up of the slow diffusive framework reorientations. Note that a direct proof of the connection between the hydrogen bond weakening and the speeding up of the rotation, either experimental or computational, is not yet available. It might be achieved, for instance, by carefully choosing the less structure breaking ions and comparing the rotational mobilities.

As discussed previously, at lower concentrations, the water rotational mobility was dominated by PWB while higher concentrations BPT water. At lower concentrations, the average number of water−water hydrogen bonds on a PWB water molecule, as presented in Figure 4, decreases slightly with the concentration, which should, in addition to the hydrogen bond weakening effect, further increase the water rotational mobility. At higher concentrations, the BPT water becomes dominant and water rotation is significantly hindered by the ion assemblies. This thus suggests that the balance between the hydrogen bond weakening effects of the ions and the confining effect of the assemblies causes the non-monotonic concentration dependence of the water rotational mobility.

The anisotropic rotation was found for the rotation of water in the cation shell, especially for the cation with small size.[71] Cations mainly slow down the reorientation dynamics of the water around the dipole vector, and anions mainly slow down the reorientation dynamics around the hydroxyl group that points toward the anion.[71] This phenomenon is also found, in the current study, for the rotation for the PB water at low concentrations (Figure 9). The rotation correlation function along the hydroxyl bond direction decays a little faster than that along the dipole direction.

Most of the thiocyanate ions are fully solvated at lower concentrations (Figure 6). The state residence times of IB and PWB SCN^- are all longer than the corresponding rotational correlation times (Table 5), which makes it meaningful to discuss the environment-dependent rotation. The rotations of PWB SCN^- are strongly correlated with the surrounding waters at low concentration while moving slightly slower due to their bigger sizes;[73−75] thus, an insignificant speeding up is observed at lower concentrations. At medium concentrations or higher, most SCN^- and K^+ form ion assemblies and the size of the ion assembly increases with concentration (Figures 5 and 6). The ratio of PB SCN^- increases and the average rotational correlation time of SCN^- decreases with concentration.

The concentration dependences of translational mobilities for different components in Figure 11 appear to be less deviated compared with the rotation in Figures 9 and 12. It has been demonstrated in the systems such as the aqueous solution of organic and biological molecules, the confined water system, and the supercooled water solutions[86−89] that the "collisional" hindrance or confining effect of the solute has a much stronger effect on the translation than the rotation. The translational motions of different components thus have much stronger correlations with each other. With increasing concentration, the ion assemblies have larger sizes, slower motions, and more water molecules confined with them (Figure 6). The confining effect thus retards the translation of water significantly, while their rotational motion is less affected by the adjacent ions, as indicated by the rather minor differences among the different subspecies of water in Figure 9B.

As a demonstration of this difference, the relative rotational correlation time and diffusion constants of water molecules at different concentrations are presented in Figure 12. The translation of water coincides with the experimentally measured viscosity, which contains the information of the average structure relaxation. The rotational mobility, on the other hand, significantly deviates from the average relaxation trend.

The time-dependent mean square displacements $T(t)$ of the PWB water at the different concentrations (Figure 13) further reveals the hindering effect of the ion assemblies on the translational motions of the water molecules. Within the first 0.3 ps, due to the similar librational motions, all of the curves increase almost identically. At longer time scale, the $T(t)$ in pure water increases linearly, since the system is fairly isotropic. PWB water molecules in 0.5 and 1.0 mol/kg solutions behave almost the same as in the pure water with only a slight augmentation. This is because there are only a small amount of ion assemblies at the lower concentrations, the collision and confinement with the ion assemblies are rare, while the hydrogen bond weakening effect of the ions slightly speed up the movement. As the concentration further increases, collision of the target PWB water with the ion assemblies happens more frequently and the confining effect is more significant; thus, the

dx.doi.org/10.1021/jp400441e | J. Phys. Chem. B 2013, 117, 2992−3004

$T(t)$ curves become more nonlinear and deviate further from the pure water line.

The information of the translational mobilities discussed above is not contained in the ultrafast infrared measurements. However, a recent work on the optical Kerr effect (OKE) and dielectric relaxation (DR) spectroscopy of the $MgCl_2$ aqueous solution[72] suggested that the OKE signal does contain the information of the water translational motion, and the difference in the concentration dependence of OKE and DR signals of $MgCl_2$ solutions can be traced back to a decoupling of translational and rotational motions of water molecules, similar to what was observed in the current work. Although the microscopic physics behind these spectroscopic observations still need to be carefully studied, this evidence points to the picture that the ion assembly causes experimentally observable dynamical phenomena in the ionic solutions.

A further issue is whether the observed neighboring of cation−anion is completely caused by thermal fluctuation, or at least partly due to other energetic reasons such as ion pairing.[1] The shorter pair residence times of water−SCN than water−water in Figure 5 and the broader distribution for the hydrogen bonds of water−SCN than those of water−water in Figure 3 suggest that the association between the SCN^- and water is weaker than that between water molecules. The residence times of SCN^- in the K^+ shell are longer than those for the other pairs in Table 5. Thus, SCN^- and K^+ have a strong tendency to pair with each other in the solution. The assembly analysis and radial distribution functions of ion pairs (Figures 2, 5, and 6) in water solutions also suggest an energetic preference of ion pairing in KSCN aqueous solutions. Our simulations thus suggest that ion pairing plays an important role in the observed neighboring of cation−anion. Additionally, a recent ultrafast infrared measurement on the NH_4SCN aqueous solution demonstrates that, even at a fairly low concentration, the probability of SCN−NH_4 pairing is 18 times higher than the SCN−water pairing. Thus, the assembling in this sort of ionic solutions is highly unlikely to be completely caused by the thermal fluctuation, which is consistent with our observations.[90,91]

There are higher first association peaks for the radial distribution functions of the K−I ion pairs than the corresponding ones of ion−water radial distribution functions in Figure 2, which indicates that the I^- also prefer to stay in the ion assemblies with K^+ like SCN^-. This is consistent with the prediction by viscosity B-coefficients.[84,85] Comparatively, the K−F ion pair prefers to form SSIP structure, given a higher and broader peak in the range 4−6 Å than the CIP characteristic peak at 2.7 Å (Figure 2). In the mixed solution of KSCN:KF:water or KSCN:KI:water, more SCN^- anions stay in the ion assemblies due to the additional KF or KI than the pure KSCN (10 mol/kg) solution. The big difference between the ratio of F^- and I^- in ion assemblies suggests that the F^- anions have a higher water affinity than I^-. Comparison of the diffusion constant and the rotational correlation times shows that KF can remarkably retard the mobility of KSCN solution and I^- plays a similar role as SCN^- and the additional KI like concentration effect of KSCN.

In conclusion, our molecular dynamics simulations suggest that the ion assembling in the KSCN aqueous solutions, which is largely induced by the ion pairing effect, can cause a significant deviation from the Stokes−Einstein behavior for the rotational dynamics. The deviations are detectable by the ultrafast infrared spectroscopy. The rotation and translation of the water molecules have different concentration dependences due to translation's higher sensitivity to the confining effect of the ion assemblies. The mobility of SCN^- is mainly determined by the size of the ion assembly and characteristic of concerted motion with ion assemblies. The non-monotonic concentration dependence of microscopic mobility results from the competition between the hydrogen bond weakening due to the weak interaction of water−SCN^- and water−K^+, and the retardation due to the confining effect of the ion assemblies.

AUTHOR INFORMATION

Corresponding Author

*E-mail: wzhuang@dicp.ac.cn (W.Z.); gaoyq@pku.edu.cn (Y.Q.G.); junrong@rice.edu (J.Z.).

Notes

The authors declare no competing financial interest.

ACKNOWLEDGMENTS

This material is based upon work supported by the NSFC QingNian Grant 21003117, NSFC key Grant 21033008, and Science and Technological Ministry of China Grant 2011YQ09000505. Y.Q.G. thanks NSFC for support (21125311 and 91027044). J.Z. gratefully thanks the support of Welch foundation C-1752, the AFOSR Award FA9550-11-1-0070, and the David and Lucile Packard Foundation. We also thank Prof. TianYing Yan in NanKai University for the extensive discussion on the manuscript.

REFERENCES

(1) Marcus, Y.; Hefter, G. Ion Pairing. *Chem. Rev.* **2006**, *106*, 4585−4621.

(2) Marcus, Y. Effect of Ions on the Structure of Water: Structure Making and Breaking. *Chem. Rev.* **2009**, *109*, 1346−1370.

(3) Ohtaki, H.; Radnai, T. Structure and Dynamics of Hydrated Ions. *Chem. Rev.* **1993**, *93*, 1157−1204.

(4) Inman, D.; Lovering, D. G. *Ionic Liquids*; Plenum Press: New York, London, 1981.

(5) Ball, P. Water as an Active Constituent in Cell Biology. *Chem. Rev.* **2008**, *108*, 74−108.

(6) Debye, P.; Hückel, E. The Theory of Electrolytes I. The Lowering of the Freezing Point and Related Occurrences. *Z. Phys.* **1923**, *24*, 185−206.

(7) Kjellander, R. Distribution Function Theory of Electrolytes and Electrical Double Layers: Charge Renormalisation and Dressed Ion Theory. *NATO Sci. Ser., II* **2003**, *46*, 317−364.

(8) Xiao, T.; Song, X. A Molecular Debye-Huckel Theory and Its Applications to Electrolyte Solutions. *J. Chem. Phys.* **2011**, *135*, 104104−104114.

(9) Nostro, P. L.; Ninham, B. W. Hofmeister Phenomena: An Update on Ion Specificity in Biology. *Chem. Rev.* **2012**, *112*, 2286−2322.

(10) Omta, A. W.; Kropman, M. F.; Woutersen, S.; Bakker, H. J. Negligible Effect of Ions on the Hydrogen-Bond Structure in Liquid Water. *Science* **2003**, *301*, 347−349.

(11) Skinner, J. L. Following the Motions of Water Molecules in Aqueous Solutions. *Science* **2010**, *328*, 985−986.

(12) Tielrooij, K. J.; Garcia-Araez, N.; Bonn, M.; Bakker, H. J. Cooperativity in Ion Hydration. *Science* **2010**, *328*, 1006−1009.

(13) Chandra, A. Effects of Ion Atmosphere on Hydrogen-Bond Dynamics in Aqueous Eectrolyte Solutions. *Phys. Rev. Lett.* **2000**, *85*, 768−771.

(14) Carrillo-Tripp, M.; Saint-Martin, H.; Ortega-Blake, I. A Comparative Study of the Hydration of Na^+ and K^+ with Refined Polarizable Model Potentials. *J. Chem. Phys.* **2003**, *118*, 7062−7073.

(15) Mancinelli, R.; Botti, A.; Bruni, F.; Ricci, M. A.; Soper, A. K. Perturbation of Water Structure due to Monovalent Ions in Solution. *Phys. Chem. Chem. Phys.* **2007**, *9*, 2959−2967.
(16) (a) Jungwirth, P.; Tobias, D. J. Specific Ion Effects at the Air/Water Interface. *Chem. Rev.* **2006**, *106*, 1259−1281. (b) Rembert, K. B.; Paterová, J.; Heyda, J.; Hilty, C.; Jungwirth, P.; Cremer, P. S. The Molecular Mechanisms of Ion-Specific Effects on Proteins. *J. Am. Chem. Soc.* **2012**, *134*, 10039−10046.
(17) Chang, T. M.; Dang, L. X. Recent Advances in Molecular Simulations of Ion Solvation at Liquid Interfaces. *Chem. Rev.* **2006**, *106*, 1305−1322.
(18) Wynne, K.; Hunt, N. T. Ultrafast Chemical Dynamics. *Phys. Chem. Chem. Phys.* **2012**, *14*, 6154−6155.
(19) Lin, K.; Zhou, X. G.; Luo, Y.; Liu, S. L. The Microscopic Structure of Liquid Methanol from Raman Spectroscopy. *J. Phys. Chem. B* **2010**, *114*, 3567−3573.
(20) Fayer, M. D.; Moilanen, D. E.; Wong, D.; Rosenfeld, D. E.; Fenn, E. E.; Park, S. Water Dynamics in Salt Solutions Studied with Ultrafast Two-Dimensional Infrared (2D IR) Vibrational Echo Spectroscopy. *Acc. Chem. Res.* **2009**, *42*, 1210−1219.
(21) Luzar, A.; Chandler, D. Hydrogen-Bond Kinetics in Liquid Water. *Nature* **1996**, *379*, 55−57.
(22) Loparo, J. J.; Roberts, S. T.; Tokmakoff, A. Multidimensional Infrared Spectroscopy of Water. II. Hydrogen Bond Switching Dynamics. *J. Chem. Phys.* **2006**, *125* (194522), 1−12.
(23) Sciortino, F.; Geiger, A.; Stanley, H. E. Effect of Defects on Molecular Mobility in Liquid Water. *Nature* **1991**, *354*, 218−221.
(24) Laage, D.; Hynes, J. T. On the Residence Time for Water in a Solute Hydration Shell: Application to Aqueous Halide Solutions. *J. Phys. Chem. B* **2008**, *112*, 7697−7701.
(25) Xu, H.; Berne, B. J. Hydrogen-Bond Kinetics in the Solvation Shell of a Polypeptide. *J. Phys. Chem. B* **2001**, *105*, 11929−11932.
(26) Pitzer, K. S. *Activity Coefficients in Electrolyte Solutions*; CRC Press: Boca Raton, FL, 1991.
(27) Pitzer, K. S.; Mayorga, G. Thermodynamics of Electrolytes. III. Activity and Osmotic Coefficients for 2−2 Electrolytes. *J. Solution Chem.* **1974**, *3*, 539−546.
(28) Sutherland, W. XVIII. Ionization, Ionic Velocities, and Atomic Sizes. *Philos. Mag.* **1902**, *3*, 161−177.
(29) Bjerrum, N. *Z. Elektrochem.* **1918**, *24*, 300−321.
(30) Arrhenius, S. Z. Ueber die Dissociation der im Wasser gelösten Stoffe. *Phys. Chem.* **1887**, *1*, 631−648.
(31) Fuoss, R. M. Conductimetric Determination of Thermodynamic Pairing Constants for Symmetrical Electrolytes. *Proc. Natl. Acad. Sci. U.S.A.* **1980**, *77*, 34−38.
(32) Oelkers, E. H.; Helgeson, H. C. Multiple Ion Association in Supercritical Aqueous Solutions of Single Electrolytes. *Science* **1993**, *261*, 888−891.
(33) Johnson, K. S.; Pytkowicz, R. M. Ion Association and Activity Coefficients in Multicomponent Solutions. In *Activity Coefficients on Electrolyte Solutions*; Pytkowicz, R. M., Ed.; CRC Press, Inc.: Boca Raton, FL, 1979.
(34) Dillon, S. R.; Dougherty, R. C. NMR Evidence of Weak Continuous Transitions in Water and Aqueous Electrolyte Solutions. *J. Phys. Chem. A* **2003**, *107*, 10217−10220.
(35) Georgalis, Y.; Kierzek, A. M.; Saenger, W. Cluster Formation in Aqueous Electrolyte Solutions Observed by Dynamic Light Scattering. *J. Phys. Chem. B* **2000**, *104*, 3405−6.
(36) Patra, M.; Karttunen, M. Systematic Comparison of Force Fields for Microscopic Simulations of NaCl in Aqueous Solutions: Diffusion, Free Energy of Hydration, and Structural Properties. *J. Comput. Chem.* **2004**, *25*, 678−689.
(37) Koneshan, S.; Rasaiah, J. C. Computer Simulation Studies of Aqueous Sodium Chloride Solutions at 298 and 683 K. *J. Chem. Phys.* **2000**, *113*, 8125−8137.
(38) Chowdhuri, S.; Chandra, A. Molecular Dynamics Simulations of Aqueous NaCl and KCl Solutions: Effects of Ion Concentration on the Single-Particle, Pair, and Collective Dynamical Properties of Ions and Water Molecules. *J. Chem. Phys.* **2001**, *115*, 3732−3741.
(39) Sherman, D. M.; Collings, M. D. Ion Association in Concentrated NaCI Brines from Ambient to Supercritical Conditions: Results from Classical Molecular Dynamics Simulations. *Geochem. Trans.* **2002**, *3*, 102−107.
(40) Degrève, L.; da Silva, F. L. B. Structure of Concentrated Aqueous NaCl Solution: A Monte Carlo Study. *J. Chem. Phys.* **1999**, *110*, 3070−3078.
(41) Degrève, L.; da Silva, F. L. B. Large Ionic Clusters in Concentrated Aqueous NaCl Solution. *J. Chem. Phys.* **1999**, *111*, 5150−5157.
(42) Fennell, C. J.; Bizjak, A.; Vlachy, V.; Dill, K. A. Ion Pairing in Molecular Simulations of Aqueous Alkali Halide Solutions. *J. Phys. Chem. B* **2009**, *113*, 6782−6792.
(43) Chen, A. A.; Pappu, R. V. Quantitative Characterization of Ion Pairing and Cluster Formation in Strong 1:1 Electrolytes. *J. Phys. Chem. B* **2007**, *111*, 6469−6478.
(44) Bian, H. T.; et al. Ion Clustering in Aqueous Solutions Probed with Vibrational Energy Transfer. *Proc. Natl. Acad. Sci. U.S.A.* **2011**, *108*, 4737−4742.
(45) Bian, H.; Li, J.; Zhang, Q.; Chen, H.; Zhuang, W.; Gao, Y.; Zheng, J. Ion Segregation in Aqueous Solutions. *J. Phys. Chem. B* **2012**, *116*, 14426−14432.
(46) Einstein, A. *Investigations on the Theory of the Brownian Motion*; Dover: New York, 1956.
(47) Debye, P. *Polar Molecules*; Dover: New York, 1929.
(48) Berendsen, H. J. C.; Grigera, J. R.; Straatsma, T. P. J. The Missing Term in Effective Pair Potentials. *Phys. Chem.* **1987**, *91*, 6269−6271.
(49) (a) Dang, L. X. Mechanism and Thermodynamics of Ion Selectivity in Aqueous. Solutions of 18-Crown-6 Ether: A Molecular Dynamics Study. *J. Am. Chem. Soc.* **1995**, *117*, 6954−6960. (b) Dang, L. X. Fluoride-Fluoride Association in Water from Molecular Dynamics Simulations. *Chem. Phys. Lett.* **1992**, *200*, 21−25. (c) Dang, L. X.; Garrett, B. C. Photoelectron Spectra of the Hydrated Iodine Anion from Molecular Dynamics Simulations. *J. Chem. Phys.* **1993**, *99*, 2972−2977.
(50) Lee, S. H.; Rasaiah, J. C. Molecular Dynamics Simulation of Ion Mobility. 2. Alkali Metal and Halide Ions Using the SPC-E Model for Water at 25 °C. *J. Phys. Chem.* **1996**, *100*, 1420.
(51) Horinek, D.; Mamatkulov, S. I.; Netz, R. R. Rational Design of Ion Force Fields Based on Thermodynamic Solvation Properties. *J. Chem. Phys.* **2009**, *130*, 124507−21.
(52) Andersen, H. C. Rattle: A "Velocity" Version of the Shake Algorithm for Molecular Dynamics Calculations. *J. Comput. Phys.* **1983**, *52*, 24−34.
(53) Allen, M. P.; Tildesley, D. J. *Computer Simulation of Liquids*; Clarendon Press: Oxford, U.K., 1987.
(54) Nosé, S. A Molecular Dynamics Method for Simulations in the Canonical Ensemble. *Mol. Phys.* **1984**, *52*, 255−268.
(55) Hoover, W. G. Canonical Dynamics: Equilibrium Phase-Space Distributions. *Phys. Rev. A* **1985**, *31*, 1695−1697.
(56) Berendsen, H. J. C.; Postma, J. P. M.; van Gunsteren, W. F.; DiNola, A.; Hauk, J. R. Molecular Dynamics with Coupling to an External Bath. *J. Chem. Phys.* **1984**, *81*, 3684−3690.
(57) Darden, T.; York, D.; Pedersen, L. Particle Mesh Ewald: An Nlog(N) Method for Ewald Sums in Large Systems. *J. Chem. Phys.* **1993**, *98*, 10089−10092.
(58) Ponder, J. W.; Richards, F. M. An Efficient Newton-Like Method for Molecular Mechanics Energy Minimization of Large Molecules. *J. Comput. Chem.* **1987**, *8*, 1016−1026.
(59) Mitchell, J. P.; Butler, J. B.; Albright, J. G. Measurement of Mutual Diffusion Coefficients, Densities, Viscosities, and Osmotic Coefficients for the System KSCN-H_2O at 25°C. *J. Solution Chem.* **1992**, *21*, 1115−1129.
(60) Mile, V.; Pusztai, L.; Dominguez, H.; Pizio, O. Understanding the Structure of Aqueous Cesium Chloride Solutions by Combining Diffraction Experiments, Molecular Dynamics Simulations, and Reverse Monte Carlo Modeling. *J. Phys. Chem. B* **2009**, *113*, 10760−10769.

(61) Tay, K. A.; Bresme, F. Kinetic of Hydrogen-Bond Rearrangements of Bulk Water. *Phys. Chem. Chem. Phys.* **2009**, *11*, 409−415.
(62) Impey, R. W.; Madden, P. A.; MacDonald, I. R. Hydration and Mobility of Ions in Solution. *J. Phys. Chem.* **1983**, *87*, 5071−5083.
(63) Koneshan, S.; Rasaiah, J. C.; Lynden-Bell, R. M.; Lee, S. H. Solvent Structure, Dynamics, and Ion Mobility in Aqueous Solutions at 25 °C. *J. Phys. Chem. B* **1998**, *102*, 4193−4204.
(64) Boisson, J.; Stirnemann, W. G.; Laage, D.; Hynes, J. T. Water Reorientation Dynamics in the First Hydration Shells of F^- and I^-. *Phys. Chem. Chem. Phys.* **2011**, *13*, 19895−19901.
(65) Laage, D.; Hynes, J. T. A Molecular Jump Mechanism of Water Reorientation. *Science* **2006**, *311*, 832−835.
(66) Geerke, D. P.; Oostenbrink, C.; van der Vegt, N. F. A.; van Gunsteren, W. F. An Effective Force Field for Molecular Dynamics Simulations of Dimethyl Sulfoxide and Dimethyl Sulfoxide-Water Mixtures. *J. Phys. Chem. B* **2004**, *108*, 1436−1445.
(67) Packer, K. J.; Tomlinson, D. J. Nuclear Spin Relaxation and Self-Diffusion in the Binary System, Dimethylsulphoxide (DMSO) + Water. *Trans. Faraday Soc.* **1971**, *67*, 1302−1314.
(68) Botti, A.; Pagnotta, S. E.; Bruni, F.; Ricci, M. A. Solvation of KSCN in Water. *J. Phys. Chem. B* **2009**, *113*, 10014−10021.
(69) Yang, L. J.; Fan, Y. B.; Gao, Y. Q. Differences of Cations and Anions: Their Hydration, Surface Adsorption, and Impact on Water Dynamics. *J. Phys. Chem. B* **2011**, *115*, 12456−12465.
(70) Collins, K. D.; Neilson, G. W.; Enderby, J. E. Ions in Water: Characterizing the Forces that Control Chemical Processes and Biological Structure. *Biophys. Chem.* **2007**, *128*, 95−104.
(71) Tielrooij, K. J.; van der Post, S. T.; Hunger, J.; Bonn, M.; Bakker, H. J. Anisotropic Water Reorientation around Ions. *J. Phys. Chem. B* **2011**, *115*, 12638−12647.
(72) Turton, D. A.; Hunger, J.; Hefter, G.; Buchner, R.; Wynne, K. Glasslike Behavior in Aqueous Electrolyte Solutions. *J. Chem. Phys.* **2008**, *128*, 161102−161105.
(73) Landau, L. D.; Lifshitz, E. M. *Fluid Mechanics*; Pergamon Press: Oxford, U.K., 1959.
(74) Dote, J. L.; Kivelson, D.; Schwartz, R. N. A Molecular Quasi-Hydrodynamic Free-Space Model for Molecular Rotational Relaxation in Liquids. *J. Phys. Chem.* **1981**, *85*, 2169−2180.
(75) Horng, M. L.; Gardecki, J. A.; Maroncelli, M. The Rotational Dynamics of Coumarin 153: Time-Dependent Friction, Non-Hydrodynamic Behavior, and Dielectric Friction. *J. Phys. Chem. A* **1997**, *101*, 1030−1047.
(76) Mukherjee, A.; Bagchi, B. Solvent Frictional Forces in the Rotational Diffusion of Proteins in Water. *Curr. Sci.* **2006**, *91*, 1208−1216.
(77) Mukherjee, A.; Bagchi, B. Rotational Friction on Globular Proteins Combining Dielectric and Hydrodynamic Effects. *Chem. Phys. Lett.* **2005**, *404*, 409−413.
(78) Raviv, U.; Klein, J. Fluidity of Bound Hydration Layers. *Science* **2002**, *297*, 1540−1543.
(79) Balabai, N.; Waldeck, D. H. Solute-Solvent Frictional Coupling in Electrolyte Solutions. Role of Ion Pairs. *J. Phys. Chem. B* **1997**, *101*, 2339−2347.
(80) Dutt, G. B.; Ghanty, T. K. Rotational Diffusion of Coumarins in Electrolyte Solutions: The Role of Ion Pairs. *J. Phys. Chem. B* **2003**, *107*, 3257−3264.
(81) Laage, D.; Hynes, J. T. On the Molecular Mechanism of Water Reorientation. *J. Phys. Chem. B* **2008**, *112*, 14230−14242.
(82) Zhang, X.; Zhang, Q.; Zhao, D. Hydrogen Bond Lifetime Definitions and the Relaxation Mechanism in Water Solutions. *Acta Phys.-Chim. Sin.* **2011**, *27*, 2547−2552.
(83) Laage, D.; Hynes, J. T. Do More Strongly Hydrogen-Bonded Water Molecules Reorient More Slowly? *Chem. Phys. Lett.* **2006**, *433*, 80−85.
(84) Jenkins, H. D. B.; Marcus, Y. Viscosity B-Coefficients of Ions in Solution. *Chem. Rev.* **1995**, *95*, 2695−2724.
(85) Marcus, Y. The Viscosity B-Coefficient of the Thiocyanate Anion. *J. Chem. Eng. Data* **2012**, *57*, 617−619.
(86) Nakahara, M.; Yoshimoto, Y. Hydrophobic Slowdown and Hydrophilic Speedup of Water Rotation in Supercooled Aqueous Solutions of Benzene and Phenol. *J. Phys. Chem.* **1995**, *99*, 10698−10700.
(87) Giovambattista, N.; Rossky, P. J.; Debenedetti, P. G. Effect of Pressure on the Phase Behavior and Structure of Water Confined between Nanoscale Hydrophobic and Hydrophilic Plates. *Phys. Rev. E* **2006**, *73*, 041604−14.
(88) Molinero, V.; Çağın, T.; Goddard, W. A., III. Mechanisms of Nonexponential Relaxations in Supercooled Glucose Solutions: the Role of Water Facilitation. *J. Phys. Chem. A* **2004**, *108*, 3699−3712.
(89) Russo, D.; Ollivier, J.; Teixeira, J. Water Hydrogen Bond Analysis on Hydrophilic and Hydrophobic Biomolecule Sites. *Phys. Chem. Chem. Phys.* **2008**, *10*, 4968−4974.
(90) Li, J.; Bian, H.; Chen, H.; Wen, X.; Hoang, B. T.; Zheng, J. Ion Association in Aqueous Solutions Probed through Vibrational Energy Transfers among Cation, Anion, and Water Molecules. *J. Phys. Chem. B* **2013**, DOI: 10.1021/jp3053373.
(91) Li, J.; Bian, H.; Wen, X.; Chen, H.; Yuan, K.; Zheng, J. Probing Ion/Molecule Interactions in Aqueous Solutions with Vibrational Energy Transfer. *J. Phys. Chem. B* **2012**, *116*, 12284−12294.